

# Detachment control in KSTAR with Tungsten divertor

Anchal Gupta<sup>a,\*</sup>, David Eldon<sup>b</sup>, KyuBeen Kwon<sup>a</sup>, Anthony Leonard<sup>b</sup>, Xueqiao Xu<sup>c</sup>, Menglong Zhao<sup>c</sup>, Ben Zhu<sup>c</sup>

<sup>a</sup>Oak Ridge Associated Universities, 100 ORAU Way, Oak Ridge, TN 37830, USA

<sup>b</sup>General Atomics, 3550 General Atomics Ct., San Diego, CA 92121, USA

<sup>c</sup>Lawrence Livermore National Laboratory, PO Box 808, Livermore, CA 94550, USA

## Abstract

We have demonstrated detachment control in KSTAR with the new Tungsten divertor using two different control variables. First variable is the attachment fraction calculated from 2-Point Model (2PM) using the ion saturation current density from divertor langmuir probes. Second, we used a prototype neural network surrogate model of UEDGE 2D trained on a set of about 70,000 simulations to provide a realtime estimate of heat flux at the outer divertor. We present the successful detachment control results and discuss future improvements in the control infrastructure and control variables for future burning plasma experiments.

## 1. Introduction

Burning plasma tokamaks such as ITER[1], SPARC[2], and the various DEMO concepts are estimated to exhaust very high heat flux in the Scrape-off Layer (SOL) towards the divertor target. Significant research has been carried over designing such divertors to withstand the high heat flux and ITER project has decided to use Tungsten as the divertor material. Thus, experimental reactors such KSTAR are in the process of upgrading their divertor and vessel walls to tungsten to design control systems and perform plasma studies in the presence of tungsten contamination. Even with high melting point of tungsten, it is estimated that perpendicular heat flux on the divertor should be limited to  $10\text{--}15 \text{ MW m}^{-2}$ [3] and the electron temperature at the divertor should remain within 8 eV[4] to avoid sputtering of tungsten and subsequent contamination of core plasma.

The heat flux reaching the divertor is typically reduced by puffing in impurity gases to dissipate energy and momentum of the exhaust plasma in SOL. This phenomenon is called divertor detachment. However, excessive impurity seeding could result in core contamination which not only reduces the fusion yield but can also cause cooling of core plasma resulting in collapse of H-mode or disruption of plasma confinement which can damage plasma facing components and vacuum vessel. Thus, it is important to carefully control the amount of impurity injected to keep the divertor cool while not contaminating the core plasma too much.

Divertor detachment is a fairly matured field with several different methods being demonstrated with different sensors and actuators in different experimental reactors. Radiated power control using bolometer measurements was shown in ASDEX Upgrade[5], C-III emission based radiation front control in TCV[6], divertor electron temperature control using triple-tip Langmuir probes was demonstrated in EAST[7] **ETC ETC (ADD all lat-**

**est feedback controlled experiments in other devies with different control variables here.)** At KSTAR, the detachment control has been achieved using ion saturation current from realtime langmuir probes for calculating attachment fraction,  $A_{frac}$ [8]. This approach has been previously demonstrated in JET[9], EAST[10], and DIII-D[7]. We have extended this approach in KSTAR with tungsten divertor and further tested a new prototy whole neural network surrogate model of UEDGE 2D, DivControlNN[11], for realtime heat flux estimation at the outer divertor.

This paper is organized as following. In Sec.2, we describe the experimental setup and the definition of different control variables used for detachment control. In Sec.3, we describe our experimental shots used for identifying the system and using the fitted plant model to tune a PI controller using frequency response for closed-loop stability analysis and optimization. In Sec.4, we show the results of our detachment control attempts. And finally, in Sec.5, we discuss our results, the possible improvements we can make in future, and other interesting contemporary work and ideas in the field of detachment control.

## 2. Experimental setup and control variables

The experiment was conducted on standard single lower null H-mode plasma profile with reference shot KSTAR # 35855 with the equilibrium profile as shown in Fig.1. The plasma shaping steps commences by 7s and the shot was programmed for flat-top upto 17s providing 10s long window for detachment control experiment. For heat flux control, N<sub>2</sub> gas puffing was used. The heat flux control variable was tested with several different inputs.

First, we utilized previously developed  $A_{frac}$ [8], which is defined as the ratio of measured ion saturation current to modeled (using 2PM[12]) ion saturation current assuming fully attached plasma.  $A_{frac}$  is a convenient choice of control variable which is easily available in most tokamaks and allows for cross comparison among machines. If the strike point on the diverter

\*Corresponding author

Email address: guptaa@fusion.gat.com (Anchal Gupta)

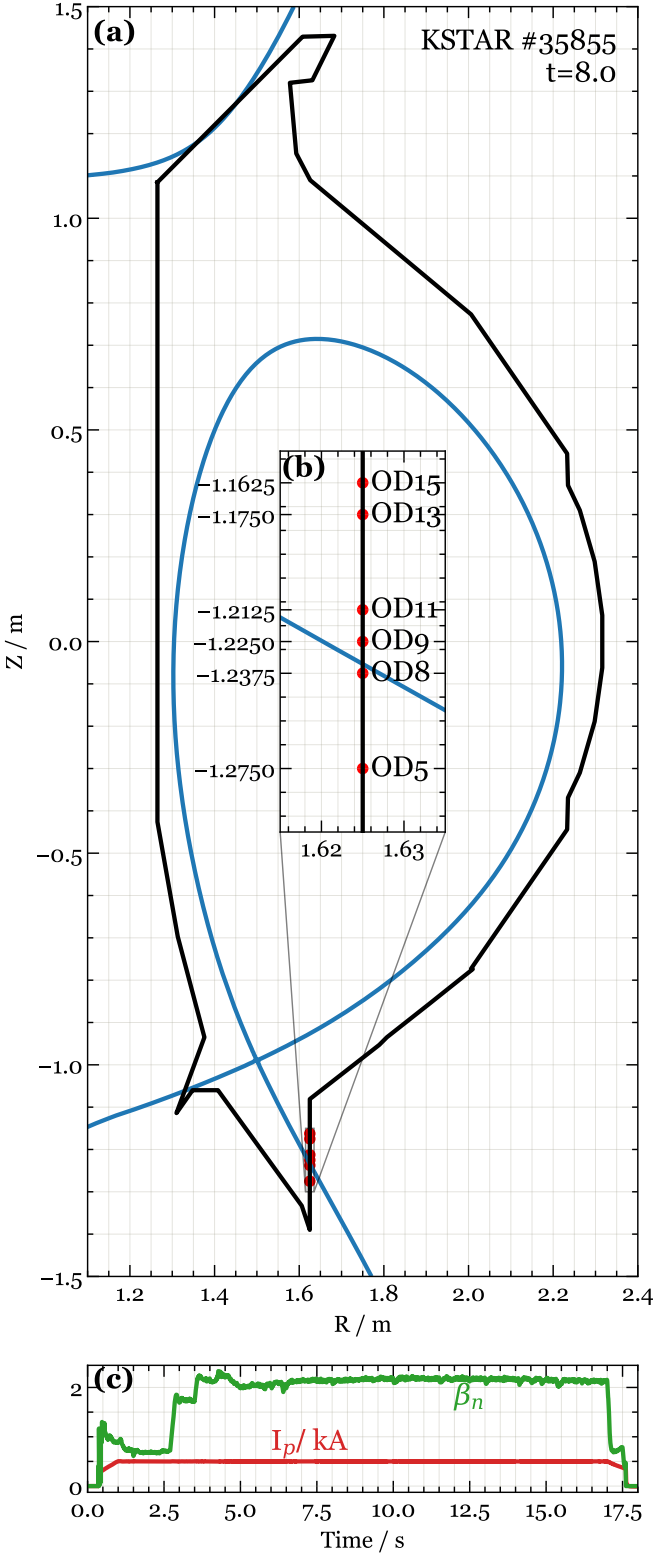


Figure 1: Reference shot # 35855. (a) Showing last closed flux surface at  $t=8$  seconds. The magnetic shape control was programmed to keep X point fixed which provided a sufficiently stable strike point on the realtime Langmuir probe array. (b) Zoomed-in locations of realtime Outer Divertor (OD) Langmuir probes. (c) Plasma current ( $I_p$ ) and  $\beta_n$  for reference shot.

tile is fixed in position well enough by the shape control system, a single close-by langmuir probe is enough to provide the ion saturation current required for  $A_{frac}$  calculation. However, if the strike point control is not good enough, or if it is required to leave it as a free variable to allow for controlling other parameters in the shape control loop (as was the case in our experiments), then it is required to estimate the true ion saturation current through measurements made by an Langmuir probe array. In our experiments, we chose the peak value from the langmuir probe array as the input to ion saturation current at strike point.

Langmuir probes would not be able to survive high heat flux in burning plasma future reactors. In general, such reactors would be severely limited in the number of realtime sensors available for control systems because of high neutron fluence and heat flux in vacuum vessel, and thus alternate control variables need to be searched for. Towards this goal, we tested a prototype of neural network surrogate model of UEDGE 2D, DivControlNN. The employed version of DivControlNN is trained on  $\approx 70,000$  UEDGE 2D simulations of KSTAR. The diffusion coefficient profile is assumed for a typical H-mode shot which can be scaled as an input to the model. The training dataset scanned core electron density ( $1.08 \times 10^{19} - 6.62 \times 10^{19} \text{ m}^{-3}$ ), plasma current (600 – 800 kA), injected total power through NBI and ECH (1 – 8 MW), impurity fraction with respect to Deuterium density (0 – 0.04), and scaling of diffusion coefficient profile with a factor (0.6 – 2). This provided a widely applicable surrogate model which gives steady state values of heat flux, ion saturation current, and electorn temperature along the two divertors, electron density and temperature at upstream point of midplane, and total radiated power, power fraction radiated from divertor, and peak radiation power location in the poloidal cross-section of the device. The model generates output within 10% error from the UEDGE 2D output.

This preliminary model, however, has been trained on UEDGE 2D simulations of KSTAR with carbon divertor and carbon as the sole impurity species. So it does not reflect the same Tungsten divertor system in which it was tested. There were several other limitations to the realtime input provided to the model. At KSTAR, the total input power from NBI and ECH sources is not completely available in realtime PCS and we had to input a feedforward signal matching the programmed rate of some sources that got summed with the other sources whose power was available in realtime. Similarly, there was no reliable input for impurity fraction in plasma and we created an adhoc gas accumulation model which measured impurity fraction by taking ratio of total puffed impurity with total puffed Deuterium gas with estimated decay rates to model the effect of pumping and wall adsorption. Finally, the diffusion coefficient scaling factor was set to 1.0 for lack of any better realtime information on it. We are in the process of training a model in Tungsten divertor environment and with gas flow rate as an input by running the simulations with multi-charge-state impurity model. This, along with improvements in realtime data availability in KSTAR would empower the model to provide outputs with higher confidence in future.

### 3. System identification and Controller Tuning

Before we attempted detachment control experiments, we took two system identification shots. The data from first system identification shot # 35853 is shown in Fig.2. In this shot, we puffed in N<sub>2</sub> gas in steps of 1.0 V, 2.5V, and 4.0 V with puff duration fo 1.5s each. A corresponding response was seen in A<sub>frac</sub>but with a delay. We later confirmed from post-shot EFIT data that the strike point was indeed within the realtime Langmuir Probe array and thus our A<sub>frac</sub>calculation was valid. We fitted the measured data with a simple first order plant model of gain K, time constant  $\tau$ , and time delay L given by:

$$G(s) = \frac{K}{\tau s + 1} e^{-Ls} \quad (1)$$

The fit resulted in identified model with K = -0.549±0.004,  $\tau$  = 1.00±0.02s, and L = 0.154±0.006s. The fit is shown in Fig.2b. Note that only the part of time series data that was used in fit is shown for the fitted curve. This fit was performed in the inter-shot interval during the experiment and has not been improved or modified after the experiment. It can be seen that A<sub>frac</sub>did not start at the value of 1.0 as should be the case for fully attached plasma initially. This was due to miscalibrated factor in PCS setting. We corrected this factor (by reducing it by factor of 2) after the system identification shot to ensure that the A<sub>frac</sub>starts at 1.0 so that controller target values make sense. This means that the identified response is high by a factor of 2 and thus we reduced the value of fitted K by factor of 2 for tuning the controller gains.

The controller gains were chosen by visualing close loop transfer function of the system with chosen PI gains as shown in Fig.3. Here, the frequency domain response of the plant model ( $G(f)$ ) and PI controller are plotted together. When connected in series, this forms the open loop transfer function of the system ( $O(f)$ ). The frequency where open loop gain becomes 1.0 is called unity gain frequency (UGF). Phase margin is defined as the additional phase delay at UGF that would make the system unstable by taking it to -180°. Additionally, we also define delay margin as the additional actuation delay that would make UGF unstable. The closed loop response is then calculated by solving the loop algebra in laplace domain:

$$C(s) = \frac{G(s)}{1 + O(s)} \quad (2)$$

Because of the large delay, we chose to not use derivative gain. The goal of tuning was to push UGF as high as possible (0.59 Hz) while keeping a reasonable phase margin (14.8 °) and margin for any additional actuation delay (69 ms). This resulted in controller settings as: K<sub>p</sub> = -10.0, T<sub>i</sub> = 253.0 ms, and  $\tau_s$  = 50.0 ms, where K<sub>p</sub> is proportional gain, T<sub>i</sub> is integral time, and  $\tau_s$  is presmoothing time constant. This is still a very aggressive choice of controller, but given that the system identification fit gave an unexpectedly high value of response time  $\tau$  = 1s probably due to too much noise during low step inputs, we decided to go ahead with this controller choice. The resulting PI controller transfer function is given by:

$$TPI(f) = K_p \left( \frac{1}{T_i s} + 1 \right) \frac{1}{1 + \tau_s s} \quad (3)$$

Unfortunately, the surrogate model was not configured properly in this system identification shot due to technical errors, so we repeated a system identification but this time we decided to keep the nitrogen valve in constant open position, to look for any deviation in the behavior. The data from this second system identification shot is shown in Fig.4. Despite all the limitations of DivControlNN as listed earlier, we still saw a good correlation in the DivControlNN heat flux output at outer divertor with the injected gas as seen in Fig.4b. This is validated by estimated A<sub>frac</sub>in Fig.4d showing that increase in detachment level as the predicted output heat flux decreases. The strike point was maintained within the realtime Langmuir Prone array (Fig.4a) validating the output of A<sub>frac</sub>. Note that we did not yet calibrate the DivControlNN model with any experimental data, so we treat the output as arbitrary units and later attempted to control the detachment with estimated changes to this arbitrary output.

We again fitted this system with a first order system with delay as described in Eq.1. The fit resulted in identified model with K = -0.302±0.004,  $\tau$  = 0.31±0.03s, and L = 0.536±0.019s. The fit is shown in Fig.4b. Here as well, the fitting shown was performed during the experiment in the inter-shot interval and has not been modified or optimized later. The time domain in which fitting curve is shown is the data where the system was fitted. Admittedly, this fit was not very good and we did not believe the lag value to be accurate. There is no physical reason for why the lag in the system would be higher when we use DivControlNN output as compared to A<sub>frac</sub>. So for the purpose of tuning the controller, we arbitrarily set the system lag value to 100 ms. The controller gains were chosen by visualing close loop transfer function of the system with chosen PI gains as shown in Fig.5 and following the same procedure as we described for A<sub>frac</sub>controller tuning. The resulting controller settings were: K<sub>p</sub> = -3.0, T<sub>i</sub> = 68.5 ms, and  $\tau_s$  = 5.0 ms creating controller given by Eq.3. Here, we estimated to achieve a UGF of 1.01 Hz, phase margin of 11.9 °, and delay margin of 33 ms. This controller was also very aggressive, but we decided to go ahead with this controller choice given the limitations of the system identification fit and lack of time for further analysis in between the allotted run time to our experiment.

### 4. Results

Utilizing the controllers tuned in Sec.3, we attempted detachment control experiments. First, we used A<sub>frac</sub>controller in KSTAR # 35857 with results shown in Fig.6. As can be seen in Fig.6a, the strike point remained within the realtime Langmuir probe array giving validity to the A<sub>frac</sub>signal shown in Fig.6b. Here, we can see that the controller was successful in closely following the target provided to it completing the pre-programmed shot length to the end. It is also evident that the aggressive control strategy was good and did not result in any long sustained oscillations while providing a quick

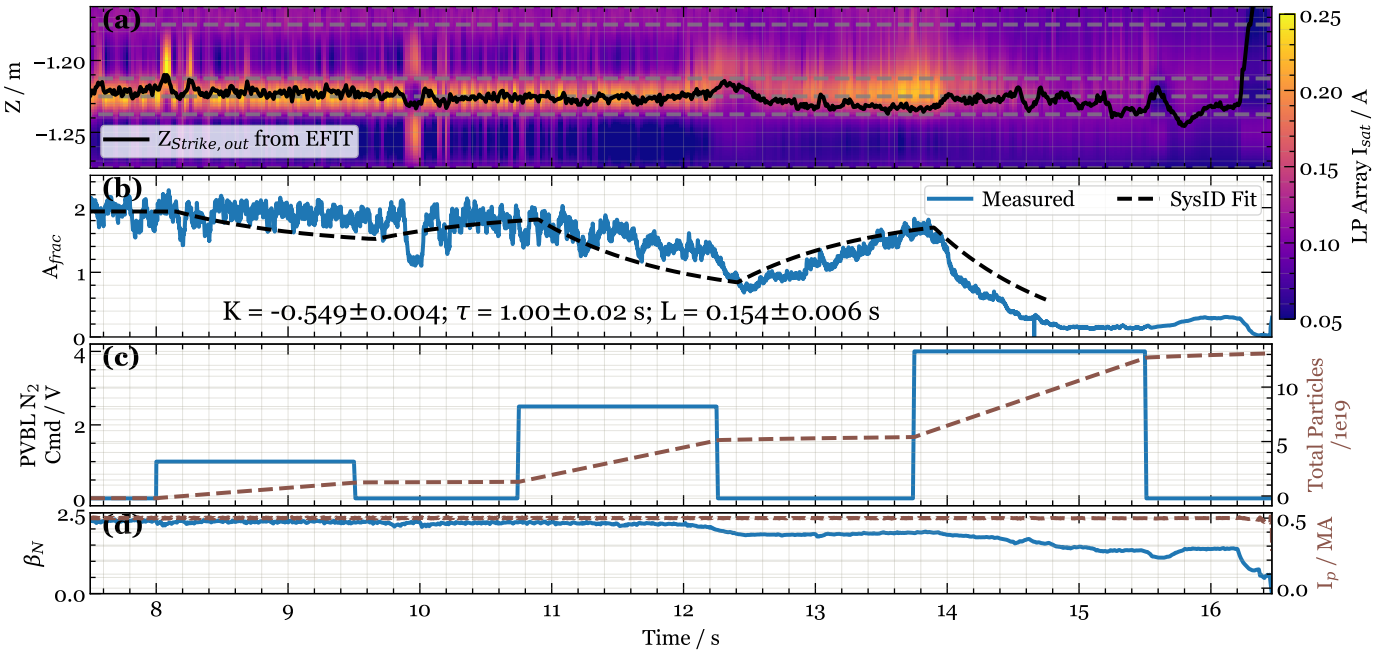


Figure 2: System identification shot # 35853. (a) Shows the measured ion saturation current by realtime Langmuir Probe array at locations marked by grey dashed lines. The data has been interpolated spatially using cubic spline interpolation. The black curve shows the post-shot calculated strike point position on outer divertor using EFIT. (b) Shows the  $A_{frac}$  calculated from peak value among the Langmuir probe array. The dashed black line shows the system identification fit on this data. (c) Left axis: Shows the  $N_2$  gas command steps sent for system identification. Right axis: Shows the cummulative  $N_2$  gas particles injected into the vessel. (d) Left axis: Shows  $\beta_N$ . Right axis: Shows the plasma current ( $I_p$ ).

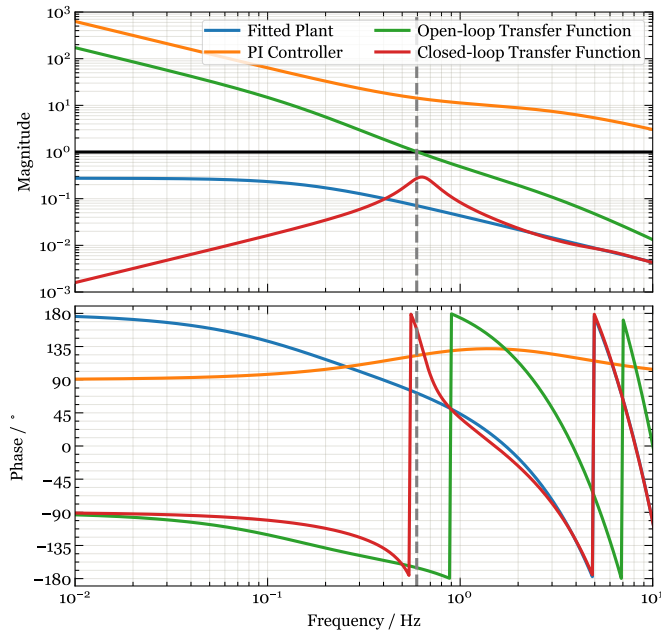


Figure 3: Closed loop transfer function analysis of the system using  $A_{frac}$  output with chosen PI controller with gains:  $K_p = -10.0$ ,  $T_i = 253.0$  ms, and  $\tau_s = 50.0$  ms.

response to the changing target value. This further validated, that  $A_{frac}$  controller strategy first devised in Ref.[8] is a viable option for detachment control even with Tungsten divertor in KSTAR.

Since  $A_{frac}$  controller has been demonstrated in the past as well, we decided to utilize remaining allotted runtime on KSTAR to test the DivControlNN prototype based controller. Fig. 7 shows the results from shot # 36161 where we deployed this controller. An immediate issue was seen with DivControlNN output that the intial heat flux calculation had a starting value than we saw in reference shots and system identification shot # 35854. Because of this, when the controller turned on at 7.5s, the large error resulted in railing of gas command output which resulted in too much  $N_2$  injected into the system. While this quickly brought down the measured signal, it also resulted in a large overshoot and probably created power starvation in the core plasma. This is evident from the system behavior in the following seconds where the calculated heat flux output did not rise much even though impurity injection was stopped. In the nest rampdown of target from 10.5s to 11.5s, more impurity was injected as we tuned an aggresive controller. It can be seen from  $A_{frac}$  in Fig. 7d that the system reached into deep detachment by this point and the ion saturation current measurements (Fig. 7a) became unreliable beyond 11s. This is why the heat flux did not naturally recover even when the target was lifted up between 13s to 15s. There is no surprise with the fact that using an uncalibrated output can result in bad set target values.

Post-shot data analysis discovered further issues in our operation of the DivControlNN model. The impurity fraction calculation as mentioned in 2 malfunctioned and sent a constant zero input to the model. Thus the model was unable to respond to large amounts of impurity that were injected into the system and was only relying on data from line integrated core electron

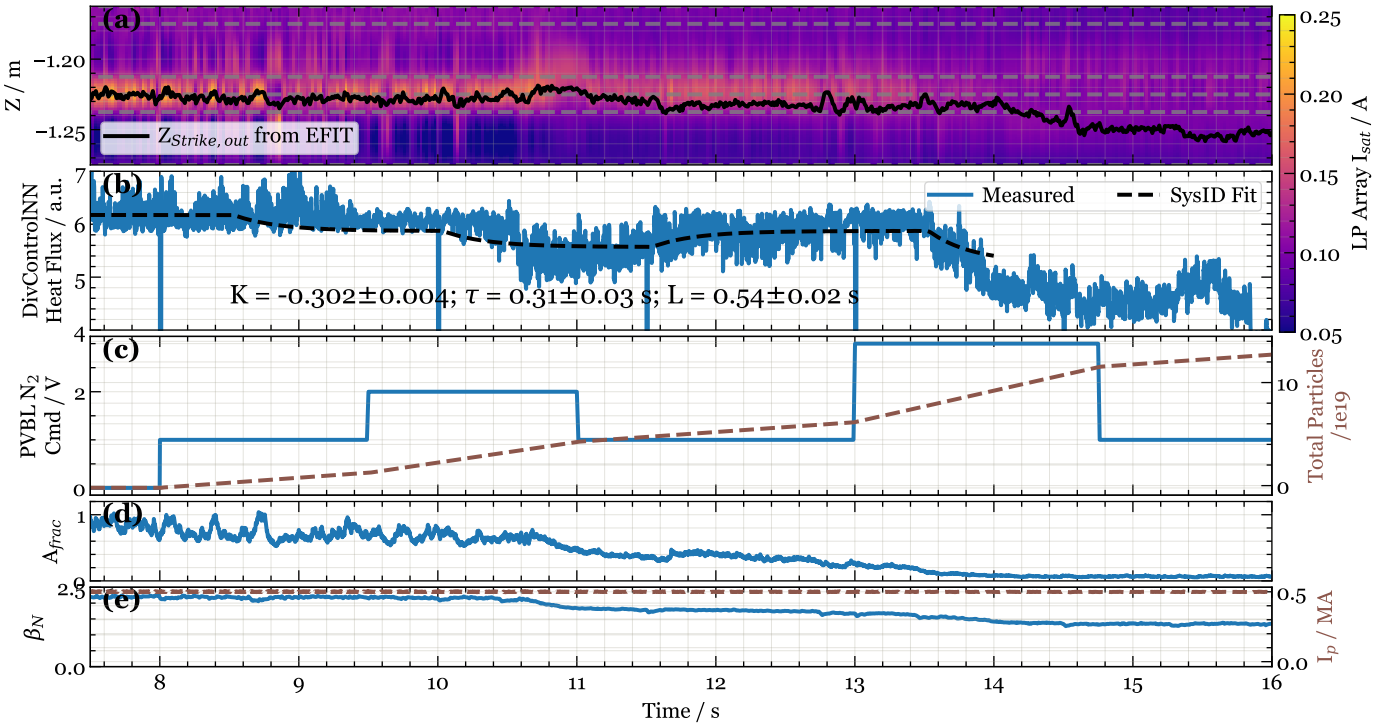


Figure 4: System identification shot # 35854. (a) Shows the measured ion saturation current by realtime Langmuir Probe array at locations marked by grey dashed lines. The data has been interpolated spatially using cubic spline interpolation. The black curve shows the post-shot calculated strike point position on outer divertor using EFIT. (b) Shows the heat flux at outer divertor calculated by DivControlNN. The dashed black line shows the system identification fit on this data. (c) Left axis: Shows the N<sub>2</sub> gas command steps sent for system identification. Right axis: Shows the cummulative N<sub>2</sub> gas particles injected into the vessel. (d) Shows the A<sub>frac</sub>calculated from peak value among the Langmuir probe array. (e) Left axis: Shows β<sub>n</sub>. Right axis: Shows the plasma current (I<sub>p</sub>).

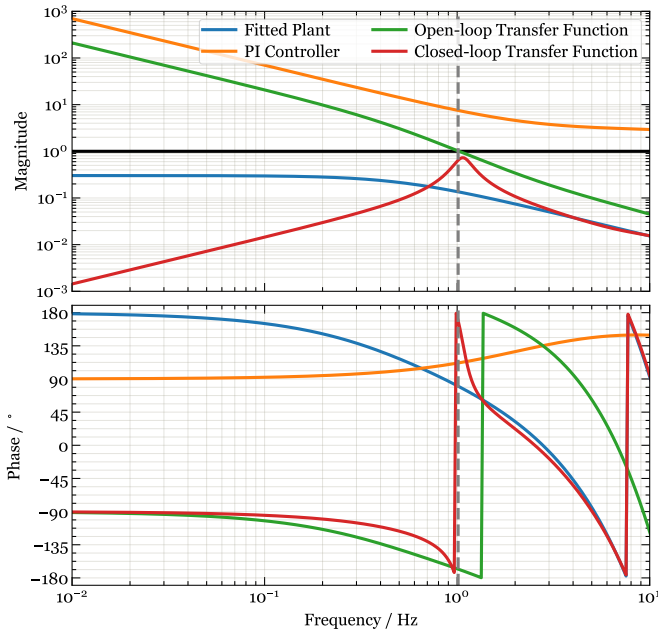


Figure 5: Closed loop transfer function analysis of the system using DivControlNN heat flux at outer divertor output with chosen PI controller with gains:  $K_p = -3.0$ ,  $T_i = 68.5$  ms, and  $\tau_s = 5.0$  ms.

density and plasma current as realtime inputs. Despite these limitations, this preliminary test sheds light on the potential of

using such a surrogate model based controller for detachment control in future reactors.

## 5. Discussion

In this paper, we described re-using A<sub>frac</sub>as a reliable control variable for detachment control provided that realtime ion saturation current measurements are available from the Langmuir probes and the strike point is controlled good enough that such an array can be used to calculate A<sub>frac</sub>. It can be seen from panels (a) and (c) in Fig.2, Fig.4, and Fig.7 that when the total injected impurity amount crosses a rough threshold of about  $1 \times 10^{20}$  particles, the plasma shape starts to rotate such that strike point on outer divertor starts drifting downwards even though the X-point is held in place by the magnetic shape control system. Thus, A<sub>frac</sub>controller is best suited with a outer strike point control system commissioned on the device which was not the case for the KSTAR experimental campaign in which we tested these controllers.

Although, langmuir probes might not be able to survive future burning plasma experiments, sacrificial probes can still be used in commissioning controllers based on other control variables in such devices given the success and reliability of this control method being demonstrated in several devices so far [NEEDCITE]. The good results from A<sub>frac</sub>controller as seen in Fig.6 could also motivate further research in similar biased electrode measurement methods of SOL plasma such as

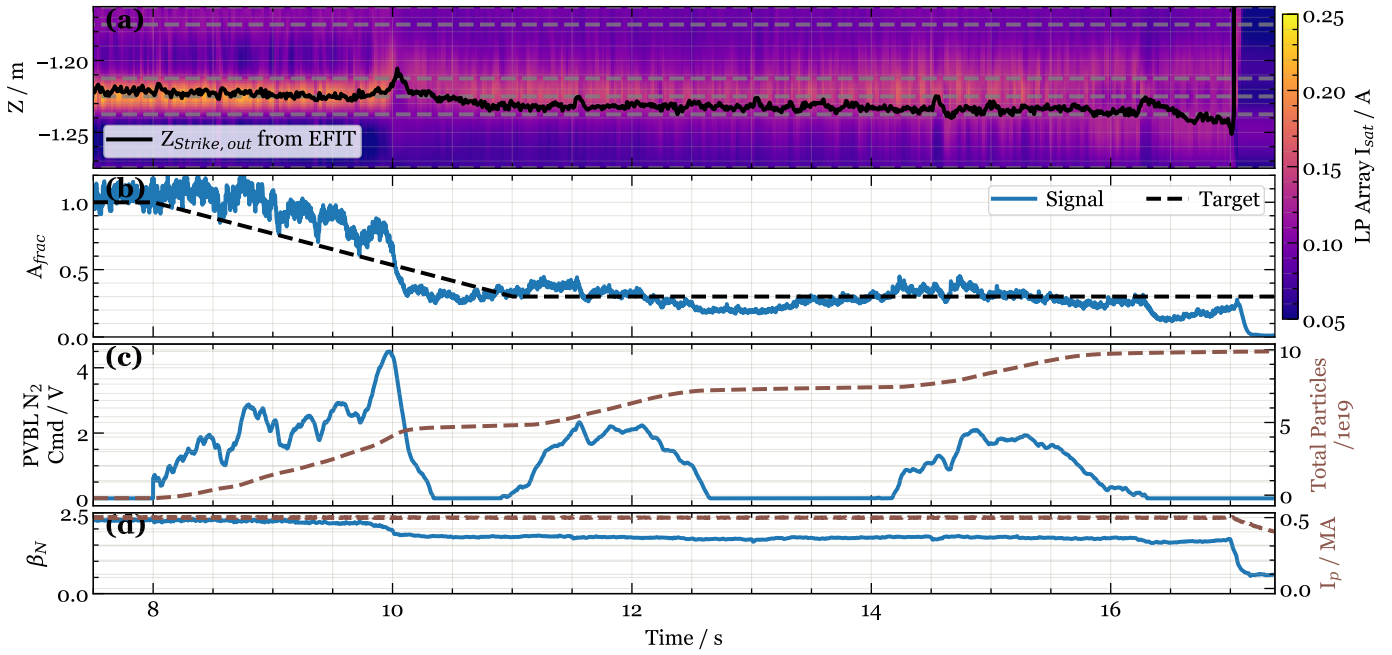


Figure 6: Detachment control shot # 35857 using  $A_{frac}$  controller. (a) Shows the measured ion saturation current by realtime Langmuir Probe array at locations marked by grey dashed lines. The data has been interpolated spatially using cubic spline interpolation. The black curve shows the post-shot calculated strike point position on outer divertor using EFIT. (b) Shows the  $A_{frac}$  calculated from peak value among the Langmuir probe array. The dashed black line shows the target provided to the controller to follow. (c) Left axis: Shows the  $N_2$  gas command steps sent for system identification. Right axis: Shows the cummulative  $N_2$  gas particles injected into the vessel. (d) Left axis: Shows  $\beta_n$ . Right axis: Shows the plasma current ( $I_p$ ).

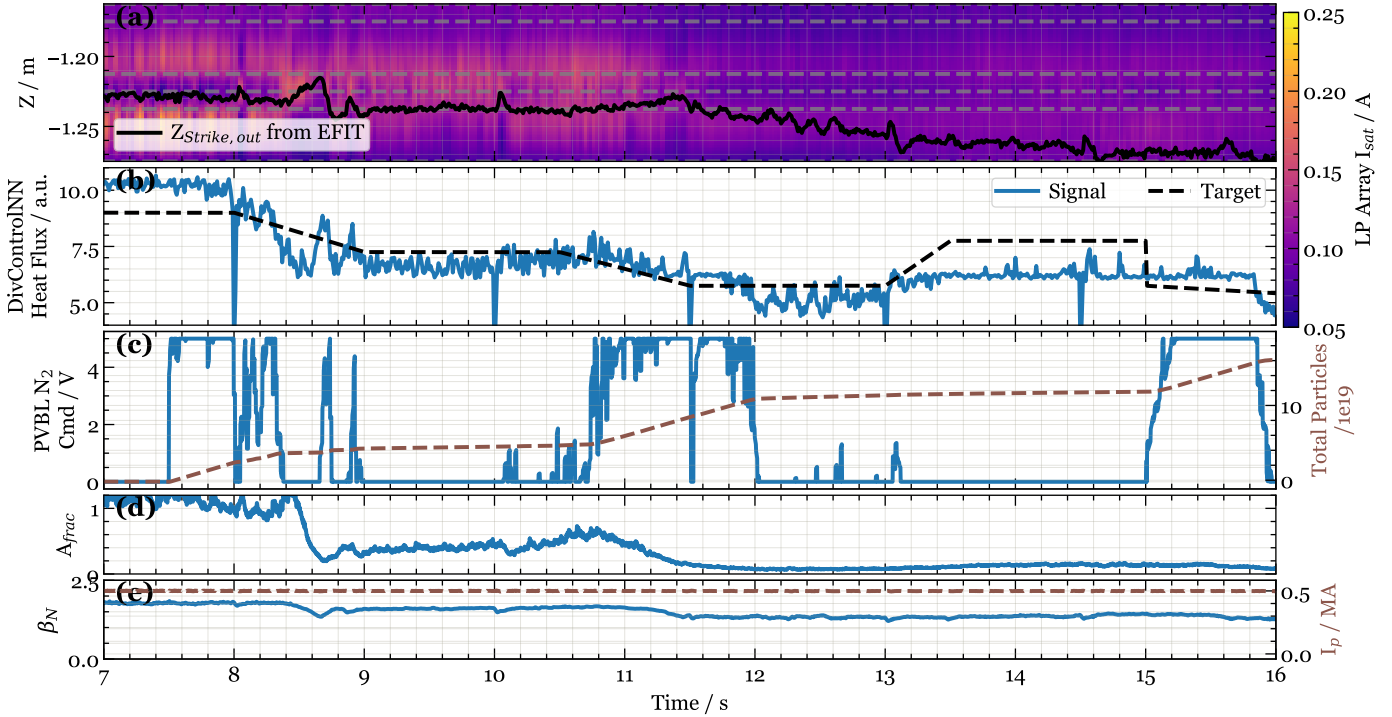


Figure 7: Detachment control shot # 36161 using DivControlNN heat flux at outer divertor. (a) Shows the measured ion saturation current by realtime Langmuir Probe array at locations marked by grey dashed lines. The data has been interpolated spatially using cubic spline interpolation. The black curve shows the post-shot calculated strike point position on outer divertor using EFIT. (b) Shows the heat flux at outer divertor calculated by DivControlNN. The dashed black line shows the target provided to the controller to follow. (c) Left axis: Shows the  $N_2$  gas command steps sent for system identification. Right axis: Shows the cummulative  $N_2$  gas particles injected into the vessel. (d) Shows the  $A_{frac}$  calculated from peak value among the Langmuir probe array. (e) Left axis: Shows  $\beta_n$ . Right axis: Shows the plasma current ( $I_p$ ).

biased divertor plates [NEEDCITE] and biased ring electrodes [NEEDCITE].

We were also able to perform a preliminary test on using DivControlNN output as a control variable for detachment control. This is an important step in the direction of achieving detachment control in future burning plasma reactors which would have very limited means of measuring the detachment level. We have identified critical weak points in the prototype of DivControlNN and the control infrastructure required to utilize this model, and we are working on improving these aspects for future tests. This further motivates focus on training surrogate models on wider set of input parameters and plasma scenarios for possible use in other control systems as well as an alternate way to provide fast diagnostic outputs in the control room during experiments for quick decision making.

Another major focus of future experiments would be to use noble gases in detachment control as N<sub>2</sub> while being optimum in cooling the SOL plasma is not allowed in burning plasma devices due to formation of tritiated ammonia that poses radioactive dangers. We are in the process of testing Ne and Ar as alternate cooling gases. More widely, there has been recent interest in using pellets for impurity injection for detachment control to reduce the large lag time and response time associated with gas puffing. Another alternative is dropping the impurity in the form of solid powder, such as Boron, although the investigation on its use for this purpose is still in preliminary phase and poses additional challenges in terms of long lag time due to free fall and accumulation of unused powder in the device.

## CRediT authorship contribution statement

## Declaration of competing interest

The authors declare that they have no known competing financial interests or personal relationships that could have appeared to influence the work reported in this paper.

## Acknowledgements

This material is based upon work supported by the U.S. Department of Energy, Office of Science, Office of Fusion Energy Sciences, under Awards DE-SC002340, and DE-AC52-07NA27344.

## Disclaimer

This report was prepared as an account of work sponsored by an agency of the United States Government. Neither the United States Government nor any agency thereof, nor any of their employees, makes any warranty, express or implied, or assumes any legal liability or responsibility for the accuracy, completeness, or usefulness of any information, apparatus, product, or process disclosed, or represents that its use would not infringe privately owned rights. Reference herein to any specific

commercial product, process, or service by trade name, trademark, manufacturer, or otherwise, does not necessarily constitute or imply its endorsement, recommendation, or favoring by the United States Government or any agency thereof. The views and opinions of authors expressed herein do not necessarily state or reflect those of the United States Government or any agency thereof.

## References

- [1] N. Holtkamp, [An overview of the iter project](#), Fusion Engineering and Design 82 (5) (2007) 427–434, proceedings of the 24th Symposium on Fusion Technology.
- [2] A. J. Creely, et al., [Overview of the sparc tokamak](#), Journal of Plasma Physics 86 (5) (2020) 865860502.
- [3] R. Pitts, et al., [Physics basis for the first iter tungsten divertor](#), Nuclear Materials and Energy 20 (2019) 100696.
- [4] S. Brezinsek, et al., [Erosion, screening, and migration of tungsten in the jet divertor](#), Nuclear Fusion 59 (9) (2019) 096035.
- [5] A. Kallenbach, et al., [Optimized tokamak power exhaust with double radiative feedback in ASDEX Upgrade](#), Nucl. Fusion 52 (2012) 122003.
- [6] T. Ravensbergen, et al., [Real-time feedback control of the impurity emission front in tokamak divertor plasmas](#), Nature Communications 12 (2021) 1105.
- [7] D. Eldon, et al., [An analysis of controlled detachment by seeding various impurity species in high performance scenarios on dIII-D and EAST](#), Nuclear Materials and Energy 27 (2021) 100963.
- [8] D. Eldon, et al., [Enhancement of detachment control with simplified real-time modelling on the KSTAR tokamak](#), Plasma Physics and Controlled Fusion 64 (7) (2022) 075002.
- [9] C. Guillemaut, et al., [Real-time control of divertor detachment in h-mode with impurity seeding using Langmuir probe feedback in jet-iter-like wall](#), Plasma Physics and Controlled Fusion 59 (4) (2017) 045001.
- [10] Q. Yuan, et al., [The first implementation of active detachment feedback control in EAST PCS](#), Fusion Engineering and Design 154 (2020) 111557.
- [11] B. Zhu, et al., Latent space mapping: Revolutionizing predictive models for divertor plasma detachment control, In Preparation.
- [12] A. W. Leonard, [Plasma detachment in divertor tokamaks](#), Plasma Physics and Controlled Fusion 60 (4) (2018) 044001.